Journal of Hazardous Materials 481 (2025) 136529

Contents lists available at ScienceDirect

Journal of Hazardous Materials

journal homepage: www.elsevier.com/locate/jhazmat

Short-term polystyrene nanoplastic exposure alters zebrafish male and female germline and reproductive outcomes, unveiling pollutant-impacted molecular pathways

Gala Pujol [a,b], Laia Marín-Gual [a,b], Laura González-Rodelas [a,b], Lucía Álvarez-González [a,b], François Chauvigné [b,c], Joan Cerdà [b,c], Mariana Teles [a], Nerea Roher [a,b], Aurora Ruiz-Herrera [a,b,*]

[a] Departament de Biologia Cel·lular, Fisiologia i Immunologia, Universitat Autònoma de Barcelona, Cerdanyola del Vallès 08193, Spain
[b] Institut de Biotecnologia i Biomedicina, Universitat Autònoma de Barcelona, Cerdanyola del Vallès 08193, Spain
[c] Institute of Marine Sciences, Spanish National Research Council (CSIC), 08003 Barcelona, Spain

HIGHLIGHTS

- Acute short-term exposure to polystyrene NPs in zebrafish germ line was evaluated.
- NPs caused testicular changes, abnormal sperm clustering, and reduced sperm motility.
- Females showed changes in oocyte stages and growth upon NPs exposure.
- RNA-sequencing links nanoplastics to gene expression changes in reproduction.

GRAPHICAL ABSTRACT

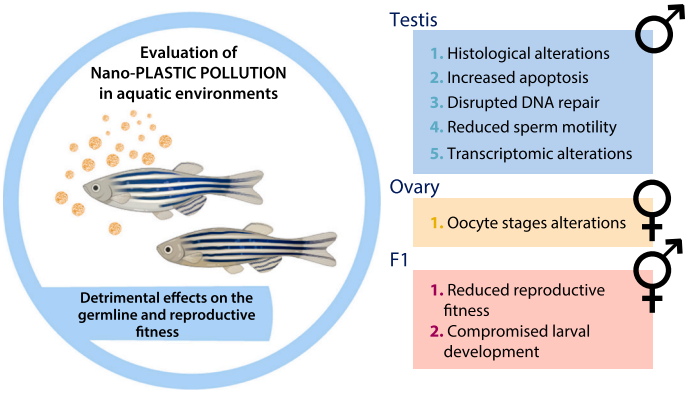

ARTICLE INFO

Key words:
Nanoplastics
Germ cells
Zebrafish
Testis
Fertility

ABSTRACT

Nanoplastics pollution is a rising environmental concern whose impacts on biodiversity and human health are far from being understood. This is particularly salient in aquatic ecosystems, where the majority of species depend on external fertilization for reproduction. Here we evaluated the effects of a short-term exposure to engineered polystyrene nanoplastics (NPs) in the zebrafish germline to further explore their impact on reproduction. To this end, zebrafish (*Danio rerio*) were exposed to 5 mg/L of 45 nm polystyrene (PS)-NPs via water for 96 h. We show that, in males, nanoplastics induced testicular histological alterations with abnormal sperm clustering and chromatin compaction, resulting in viable spermatozoa but with reduced motility. Moreover, in females we observed an alteration in oocyte stages frequencies during oogenesis, possibly reflecting alterations in oocyte growth. RNA-sequencing analysis in male testis links nanoplastic induced alterations in the expression of genes involved in chromatin structure, meiosis and DNA double-strand break formation and repair progression, and

* Corresponding author at: Departament de Biologia Cel·lular, Fisiologia i Immunologia, Universitat Autònoma de Barcelona, Cerdanyola del Vallès 08193, Spain.
E-mail address: aurora.ruizherrera@uab.cat (A. Ruiz-Herrera).

https://doi.org/10.1016/j.jhazmat.2024.136529
Received 4 September 2024; Received in revised form 29 October 2024; Accepted 13 November 2024
Available online 15 November 2024

gametes recognition. Flow cytometry analysis revealed that the observed effects in males were directly due to nanoplastics penetrating the testicular barrier and being internalized within germline cells. Overall, our results demonstrate that acute exposure to NPs can compromise reproductive fitness, underscoring the environmental and health impacts of NPs pollution.

1. Introduction

Understanding how species can respond and adapt to environmental cues is essential for preserving biodiversity. This is especially relevant in the Anthropocene era, which is characterized by the pervasive presence of pollutants in the environment, including oceans, rivers, and soils. Among all pollutants, synthetic plastics represent one of the most concerning threats to biodiversity and fauna reproductive health. Both marine and terrestrial species are continually exposed to both micro- (MPs, particles with diameters less than 5 mm) and nanoplastics (NPs, non-natural polymers less than 1000 nm) [1]. These particles have become environmentally pervasive, with aquatic ecosystems being particularly susceptible to their accumulation. Therefore, there is an urgent need to investigate the disruptive effects of NPs at multiple levels: organisms, tissues, and cells.

Due to their smaller size, physico-chemical features, bioavailability and transport activities, the hazardous effects of NPs may be potentially more harmful for organisms than those of MPs. Additional impacts may arise from plastic additives and organic pollutants also present in the environment, that may be adsorbed on the NPs surface, a phenomenon called the 'Trojan horse effect' [2-4]. The primary detrimental effects of NP particles are attributed to their potential for bioaccumulation and biomagnification, owing to their environmental persistence. In fact, NP particles can traverse numerous biological barriers and directly interact with their cellular machinery having an impact at the cellular and subcellular levels [5]. Yet, the underlying molecular mechanisms remain largely unexplored, especially when considering the germline. To address this, we present an in vivo investigation into the fertility impacts of polystyrene nanoplastics (PS-NPs) on zebrafish germline and progeny.

Germ cells represent a unique cell model, where unipotent diploid cells (gonia) undergo extensive cellular differentiation (gametogenesis) to form highly differentiated cells (oocytes and sperm) that ultimately form a totipotent embryo. This complex process is divided into three stages: (i) proliferation and differentiation of gonia; (ii) meiosis, a reductional division that produces haploid cells through two consecutive cell divisions (meiosis I and meiosis II); and (iii) differentiation into round spermatids that are transformed into densely compacted spermatozoa during spermiogenesis in the case of males. In teleost fishes, oogenesis is a dynamic process and occurs continuously in the ovary of zebrafish and can be divided into four major phases: (i) oogonia proliferation and transformation into a primary oocyte (PO); (ii) primary growth or previtellogenic, from PO to the cortical alveoli stage (CA); (iii) vitellogenic period, the main feature of which is the incorporation of vitellogenin, and (iv) final stages consisting of oocyte maturation (meiosis resumption) and ovulation [6-8]. Spermatogenesis in zebrafish and other fish, on the other hand, occurs in a cystic organization in which developing germ cell syncytia including spermatogonia, primary spermatocytes, round spermatids and sperm are encapsulated by Sertoli cells [9,10].

The histological distribution of teleost fishes' testes renders germ cells especially vulnerable to the effect of environmental drivers, including temperature and pollutants, such as NPs. Yet, little is known on the effect of this pollutants on the germline and reproductive fitness of exposed individuals. Recent data in both model and non-model species suggest that NPs exert toxic effects on several aspects of reproduction, including developmental and metabolic abnormalities of offspring [11-15]. It remains unclear, however, which are the underlying cellular and molecular mechanisms responsible for the in vivo detrimental effects of NPs on males and female fertility, especially in the context of gametogenesis.

Here we present an in vivo study on the fertility costs of polystyrene (PS)-NPs (thereafter PS-NPs) in zebrafish. To that aim we combine histological analysis, sperm motility and fertility assays with RNA-seq data to decipher the molecular mechanisms underlying germline dysfunction upon acute exposure to PS-NPs. In males, we observed that NPs induced an atypical histological distribution characterized by increased clustering of germ cells and chromatin compaction within the testis. This histological effect of NPs was associated with elevated levels of germ cell apoptosis, leading to spermatozoa with diminished motility. This was accompanied by altered gene expression related to germline dysfunction in males, including genes associated with chromatin remodeling and double-strand break (DSB) formation. In females, we noted minor alterations in the frequencies of oocyte stages during oogenesis, potentially indicating subtle effects on oocyte growth. Fertility assays revealed reduced levels of accumulated survival and a delay in larvae hatching. Overall, our results provide novel insights into the molecular and reproductive effects of PS-NPs exposure in zebrafish, demonstrating for the first time that acute exposure can compromise reproductive fitness by directly altering genome structure and function as the result of a direct internalization in germ cells. These findings underscore the significant environmental and health impacts of NP pollution.

2. Material and methods

2.1. Fish maintenance

Adult wild type zebrafish (3.85 cm ± 0.50 cm total length, 0.45 g ± 0.12 g total weight) were purchased from PISCIBER (Terrassa, Barcelona, Spain). A total of 72 fish (36 males and 36 female) was randomly allocated in 15 L tanks with a re-circulating system ensuring constant water oxygenation and filtering. Males and females were kept separately in acclimatization for a period of two weeks under standard conditions as previously described [16]. Throughout the acclimation period, fish were fed daily *ad libitum* (ZM-400 fry food 5 kg, ZM Fish Food & Equipment and brine shrimps) and water parameters (temperature, pH, ammonium, nitrites, and nitrates) were monitored accordantly.

2.2. Experimental design

Fish were randomly separated into two groups: (i) Control (0 μg/L PS-NPs) and (ii) Exposed to NPs (5000 μg/L PS-NPs) (Fig. S1). For each experimental condition and sex, fish were randomly distributed in 3 different aquariums per replicate (4 L) with 6 fish per tank. After 24 h of acclimation, fish were exposed to PS-NPs for 96 h. Briefly, fresh PS-NPs were added into the water every 24 h (at 9.00 am) during 4 consecutive days. During this period, 50 % of the water tank was renewed every other day and water parameters were monitored accordingly. Animals were not fed during the exposure period as differences in food intake could alter the nanoparticle effect and animal's metabolism. All animals were monitored twice a day (9:00 am and 4:00 pm) and scored depending on their behavior. Any fish with wounds, severe floating abnormalities, or extreme disorientation were withdrawn from the experiment and evaluated. Once the 4-days exposure period elapsed, fish were individually euthanized by immersion in a lethal dose (300 mg/L) of MS-222 (CAS 886–86–2) and biopsies were taken accordantly to the downstream analyses performed (see below). All experimental procedures were carried out in accordance with animal ethics guidelines approved by University Animal Experimentation Ethics Committees

(Universitat Autònoma de Barcelona).

2.3. Nanoparticles characterization

Polystyrene (PS) polymer particles (~45–50 nm mean diameter) were commercially obtained (#PC02002, Bangs Lab., Fishers, Indiana, USA). The particles were characterized prior to the experiment in the water used in the experiment (AQ water) with no presence of biologic material, by dynamic light scattering (DLS) (Zetasizer Pro, Malvern). For this purpose, dilutions were prepared from the original stock of PS-NPs (100 mg/ml) in AQ water and hydrodynamic size, polydispersity index (PDI) and zeta potential were measured at 0 h, 24 h, 48 h, 72 h and 96 h. For hydrodynamic size we used a ZEN0040 tray with 60 µl capacity, whereas for Z potential, a DTS1070 with 1 ml capacity was used. DLS measurements showed that the hydrodynamic diameter of PS-NPs, the PDI and Z potential did not present any significant modification in the range between 0 – 96 h in aquarium water (Fig. S2A-B). Field emission scanning microscopy representative images were previously reported [17].

2.4. Gonadal sampling for histology and immunofluorescence

Testis and ovaries from both groups (control and exposed) were collected for histological and immunofluorescence procedures. Tissues were either subjected to Bouin's fixation (saturated picric acid, formalin, and glacial acetic acid at 15:5:1 proportion), or PFA 4 % (pH=7.4) fixation. After an overnight incubation for fixation, samples were dehydrated with an increasing ethanol battery and embedded in paraffin. Microtome Section (7 µm) were obtained, fixed overnight at 37 ºC into polylysine treated slides. Subsequently, slides were deparaffinized with xylol and hydrated again with a decreasing ethanol battery. Bouin's fixed samples were stained with PAS-hematoxylin (one minute hematoxylin), whereas PFA fixed gonads were subjected to immunofluorescence procedures (see below).

2.5. Histological analysis

PAS-Hematoxylin testicular and ovarian sections were captured using a microscope (Axiophot Zeiss) equipped with a camera (ProgRes® CS10plus, Jenoptik). Images were captured with 40x lens for testis and 20x and 40x lenses for ovaries and using WNK DATAGETFL program (A. Coloma, Open Microscopy). In case of males, images were analyzed using Image J to interrogate the intensity of sperm cysts. At least, 100 sperm clusters for each replicate were delimited with a polygonal selection and data was collected. The following parameters were considered: cluster area, intensity mean, intensity standard deviation, minimum intensity, maximum intensity, cluster perimeter, and intensity median. The mean intensity of each selected cluster was analyzed with RStudio. In the case of ovaries, equivalent sections from all replicates were analyzed under the microscope and the number of oocytes at each stage (I, primary growth (subdivided in IA, pre-follicle phase; IB, follicle phase); II, cortical alveolus; and III, vitellogenesis) was obtained for further statistical analysis in RStudio.

2.6. Apoptosis analysis

Immunostaining of testis samples was performed using the following antibodies: mouse anti-RNA polymerase II (#5408, Abcam, 1:200 dilution) and rabbit anti-caspase3 (#9664, Cell Signaling Technology, 1:100 dilution). Primary antibodies were detected by the following 1:200 diluted secondary antibodies: anti-mouse Cy3 in goat (#115–165-003, Jackson Immunoresearch) and anti-rabbit FITC in goat (#111–095-003, Jacksons Immunoresearch). Briefly, deparaffinized slides from PFA 4 % fixed testis were subjected to antigen retrieval. This consisted of slides being immersed in Sodium Citrate Buffer and heated for 20 min in a microwave at a medium-low temperature (~150 Watts). After a 20-minute room temperature cool down, slides were washed twice for 5 min in PBST (0.05 % Triton X-100 in 1X PBS) in agitation, and 100 µl per slide of the primary antibodies diluted in PBST was added prior to an O/N incubation at 4 ºC in a humidified chamber. Next, slides were washed twice for 5 min in PBST in agitation and 100 µl of the secondary antibodies diluted in PBST were added and slides were incubated for 1 h in a humidified chamber at 37 ºC. Thereupon, slides were washed twice in PBST and twice in 1X PBS, and DNA was counterstained with 15 µl of antifade solution (Vectahsield) containing 0.1 µg/ml DAPI and stored at −20 ºC. Slides were analyzed using an epifluorescence microscope (Axiophot, Zeiss) equipped with a camera (ProgRes CS10plus, Jenoptik) and suitable emission filters (DAPI, FITC and Cy3). Images were captured with 63x lens and using WNK DATAGETFL program (A. Coloma, Open Microscopy). The number of caspase-3 positive cells on each spermatocyte I cyst was microscopically quantified and analyzed with RStudio.

2.7. Spermatocyte spreads and immunofluorescence

Testicular biopsies were snap frozen in liquid nitrogen and stored at −80 ºC until use. Spermatocyte spreads were performed as previously reported [18-20], with modifications. Succinctly, half testicle was cut up on a slide and minced with a scalpel as 1X PBS and lypsol 1 % were added according to its original size. Once minced, cells were incubated for 20 min at RT in agitation in a humidified chamber to permit the added lypsol to swell the cells. Freshly prepared 4 % fixative solution was added to the samples and incubated for 4 h at 4 ºC in a humidified chamber. Then, slides were let dry and washed in 1 % Photo-Flo to undergo immunofluorescence procedures.

Immunostaining was performed using two primary antibodies: rabbit anti-SYCP3 (#ab15093, Abcam, 1:100 dilution) and Guinean pig anti-Dmc1 (kind gift from Yukiko Imai, 1:100 dilution). Primary antibodies were detected by the following 1:200 diluted secondary antibodies: anti-Guinean pig Cy3 in donkey (Jackson Immunoresearch) and anti-rabbit FITC in goat (#111–095-003, Jacksons Immunoresearch). Slides were washed twice in PTBG (0.05 % Tween-20 in 1X PBS) and immersed, for 1 h RT in agitation, in previously heated at 37 ºC blocking solution (1.5 % BSA, 0.5 % Triton X-100 in 1X PBS). Next, 100 µl of primary antibodies diluted in blocking solution were added to the slides and incubate O/N at 4 ºC in a humidified chamber. The next day, after two washes in PTBG, 100 µl of the secondary antibodies diluted in PTBG were added for 1 h at 37 ºC in a humidified chamber. Finally, slides were washed twice in PTBG and twice in 1X PBS prior to DNA counter staining with 15 µl of antifade solution (Vectahsield) containing 0.1 µg/ml DAPI and stored at −20 ºC until use.

2.8. DMC1 foci analysis

Dmc-1 and SYCP3 immunostained slides were analyzed under the same epifluorescence microscope (Axiophot, Zeiss) and program specified above. Prophase I spermatocytes were identified by SYCP3 expression and captured with a 63× lens. The resulting images were observed with Photoshop to quantify the number of Dmc-1 foci per cell (only Dmc-1 foci overlapping with SYCP3 were considered). Four different prophase I substages were considered: leptotene, early zygotene, late zygotene and pachytene. The results were analyzed with RStudio.

2.9. Sperm motility assay

Fresh testis were collected from control and exposed animals. Testicles were diluted and disaggregated in 50 ml of NAM (Non-Activating Medium; NaCl 62.5 mM, KCl 65 mM, $MgCl_2$ 6.5 mM, $CaCl_2$ 2.35 mM, $MgSO_4$ 1 mM, $NaHCO_3$ 10 mM, glucose 7 mM, Hepes 30 mM 0.1 % BSA; pH 7.5) and spermatozoa concentration and motility were analyzed by CASA (Computer Assisted Sperm Analysis). Samples were loaded under

a coverslip and spermatozoa concentration was evaluated. After activation by dilution in water (1:3), 1 s videotapes were obtained, and spermatozoa motility was analyzed. Both, sperm concentration and motility analysis were the result of 3 different areas analysis for each sample and aliquot, which was performed using the Integrated Semen Analysis System software (ISAS®v1, Proiser, Valencia, Spain). For sperm motility analysis, the percentage of total motile spermatozoa was recorded. Capturing settings consisted of a counting chamber ISAS R2C10 and a camera ISAS 782 C with an image resolution of 768 × 576 pixels.

2.10. Fertility assay

After exposure, 3 breeding control groups and 3 breeding exposed groups were established using a 1:2 female/male ratio (3 replicates). Breeding crosses were set at 6:00 pm, and eggs were collected the next day between 12:00 am and 2:00 pm. F1 eggs were quantified, collected, and kept in E3 (5 mM NaCl, 0.17 mM KCl, 0.33 mM $CaCl_2$, 0.33 mM $MgSO_4$) with 1 % methylene blue at 28 ºC in Petri dishes. F1 was monitored daily and data regarding different parameters was reported, including percentages of F1 mortality/viability and hatching, together with total numbers of embryo and larvae produced. All these parameters were interrogated at different timepoints: 24 h, 48 h, 54 h, 72 h, and 96 h. When present, dead individuals and debris were removed and E3 medium added accordingly.

2.11. Larvae physiology

Seven dpf (*days post-fertilization*) individuals resulting from non-exposed adult breeding aquarium (N = 11) or from PS-NPs exposed adult breeding aquarium (N = 8) were selected randomly and transferred to 96 well-plates (1 embryo/well at a density of 1 embryo/0.5 ml of E3 medium) for observation. Both heart rate and morphological development was assessed, including pericardial edema, yolk sac edema, curved notochord, and tail, as described previously [21].

2.12. Gene expression

Total testis RNA extraction was performed using TRIzol reactive (#15596026, Thermo Fisher Scientific) following manufacturer's recommended protocols. Briefly, TRIzol immersed samples were mixed and incubated for 15 min with chloroform. After, samples were centrifuged, and the aqueous phase was transferred to a new tube with isopropanol and incubated O/N at −80 ºC. The day after, samples were washed in 70 % EtOH. Then, RNA was air dried and resuspended in miliQ water. RNA concentration and integrity number (RIN) were determined using the Agilent 2100 Bioanalyzer (Agilent Technologies). Three biological repeats per condition were used for Illumina sequencing PE150 (Novogene).

Raw reads were examined for quality issues using FastQC to ensure library generation and sequencing were suitable for further analysis. By using STAR tool from Anaconda, sequenced raw reads were aligned to the NCBI zebrafish reference genome (GRCz11) to obtain their respective counts. From the resulting data RNA plots (PCA and MAplot) and differential expression at the gene level (p-value<10e-2 and fold-change>1) were called with DESeq2 RStudio package. Once differentially expressed genes were obtained, a GO FAT and a Reactome pathway analysis were performed, and terms were manually clustered after a FDR filtering (FDR<0.1).

2.13. Exposure to labeled nanoparticles

To assess plastics' bioavailability, male fish were randomly separated into two identical groups with 4 individuals each: (i) Control and (ii) Exposed to labeled NPs (5000 µg/L Dragon-Green labeled PS-NPs, #FSDG001, Bangs Laboratories) for 48 h. Conditions, parameter and animal monitoring and euthanasia were performed as detailed in Section 2.2. DLS measurements showed that the hydrodynamic diameter of labeled PS-NPs and the PDI did not present any significant modification in the range between 0 – 48 h in aquarium water (Fig. S2C-D), mirroring studies [22]. While stability could pose a challenge in long-term exposure scenarios, this was not an issue in the study due to the acute exposure period of 48 h.

2.14. Flow cytometry analysis

Following exposure, testis were freshly collected and tissue cells were individualized by disaggregation for further cytometry analysis similarly to previous reports [23]. Gonads were disaggregated by placing them in GBSS (Gey's Balanced Salt Solution) (#G9779–ml, Sigma-Aldrich), with 0.5 mg/ml of collagenase type II (#1701015, Life Technologies) and 1 ng/µl of DNase I (#DN25–10MG, Sigma-Aldrich) following an incubation of 30 min at 32 ºC. Then, 0.5 mg/ml of trypsin (#T9935–100MG, Sigma Aldrich) were added to the sample and incubated 20 min at 32 ºC. Following, trypsin was quenched by the addition of 15 % of fetal bovine serum (#10270106, Thermo-Fisher) prior to the sample filtering using a 70 µm cell strainer. In order to prepare the sample for FACS analysis (Fluorescent Activated Cell Sorting), cells were spun for 10 min at 500 g and resuspended in 1X PBS. Then, half of the sample was maintained at 32 ºC unstained, whereas the other half was stained for 1:30 h at 32 ºC with 5 µg/ml of Hoechst 33342 (#62249, Life Technologies). Cells were sorted using a BD FACSDiscover S8 Cell Sorter. The spectrum between control and exposed individuals was analyzed to assess the absence/presence of the fluorescent particle in germ cells. To do so, B2 fluorescence detector (517 nm wavelength detector, corresponding to Dragon-Green's emission peak (520 nm) was adjusted at a gain value of 34.3 (to avoid saturation) and studied. Additionally, positive and negative cells for Dragon Green were sorted by their complexity (side scatter, SSC) and fluorescence (B2, Dragon Green emission wavelength). Both groups were collected after sorting in 1X PBS. Imaging from the sorted cells was obtained using the Imaging Blue 1 (535) detector and adjusting to 66.15 its gain value. For imaging recording LightLoss (Imaging) and Dragon-Green fluorochrome detector parameters were selected. Sorted cells were then fixed into slides by incubating with freshly prepared 4 % fixative solution (PFA 4 % with 0.15 % Triton X-100, pH=9.8) for 4 h RT in a humidified chamber. After air-drying the slides, they were washed in 1 % Photo-Flo.

2.15. Germ cell enrichment analysis

Subsequent immunofluorescence staining was conducted after FACS to identify spermatogenic cellular stages (spermatogonia, spermatocytes I, round spermatids and sperm) that incorporated labeled NPs. To do so, two primary antibodies were used: rabbit anti-SYCP3 (#ab15093, Abcam, 1:100 dilution) and mouse anti-RNA polymerase II (#5408, Abcam, 1:200 dilution). To detect them, the following 1:200 diluted secondary antibodies were used: anti-rabbit FITC in goat (#111–095-003, Jacksons Immunoresearch) and anti-mouse Cy3 in goat (#115–165-003, Jackson Immunoresearch). After washing the slides twice in PTBG (0.05 % Tween-20 in 1X PBS), 100 µl of primary antibodies diluted in PTBG were added into the slides and incubated O/N at 4 ºC in a humidified chamber. Then, slides were washed twice in PTBG prior to the addition of 100 µl of the secondary antibodies diluted in PTBG and 1 h incubation at 37 ºC in a humidified chamber. Lastly, samples were washed twice in PTBG and twice in 1X PBS and DNA was counterstained with 15ul of antifade solution (Vectahsield) containing 0.1 µg/ml DAPI and stored at −20 ºC until used.

Stained slides were analyzed under the epifluorescence microscope (Axiophot, Zeiss) as detailed in Section 2.6. Cell types were distinguished according to the following features: (i) spermatogonia showed a granulated nucleus and were positive for RNA polymerase II, (ii) spermatocytes I had positive expression for both SYCP3 and RNA polymerase

II staining, (iii) round spermatids and sperm, share a similar morphology by DAPI staining, but showed distinct RNA polymerase II staining (round spermatids were positive, whereas spermatozoa were negative).

2.16. Quantification and statistical analysis

Statistical analyses were performed by a two-way ANOVA with no interactions, to isolate the real effects of the exposure from the experiment performance date or a Chi-square test when multiple variables were compared. Normality and heterogeneity tests were applied to the data residues to ensure their distribution. Statistical methods and p-values are displayed in each plot or listed in the figures.

3. Results

3.1. Acute exposure to PS-NPs affects spermatogenesis and sperm motility

We first characterized spermatogenesis progression in zebrafish testicular cysts using a set of meiotic markers on histological sections (Fig. 1A-B). Anti-SYCP3 antibody labeled axial elements of the synaptonemal complex that were used to classify primary spermatocytes following previous observations in zebrafish meiotic studies [24]. The use of the phosphorylated RNA pol II (the active form of RNA pol II) served to further distinguish between round spermatids (middle signal levels) and sperm (absence of RNA pol II signal).

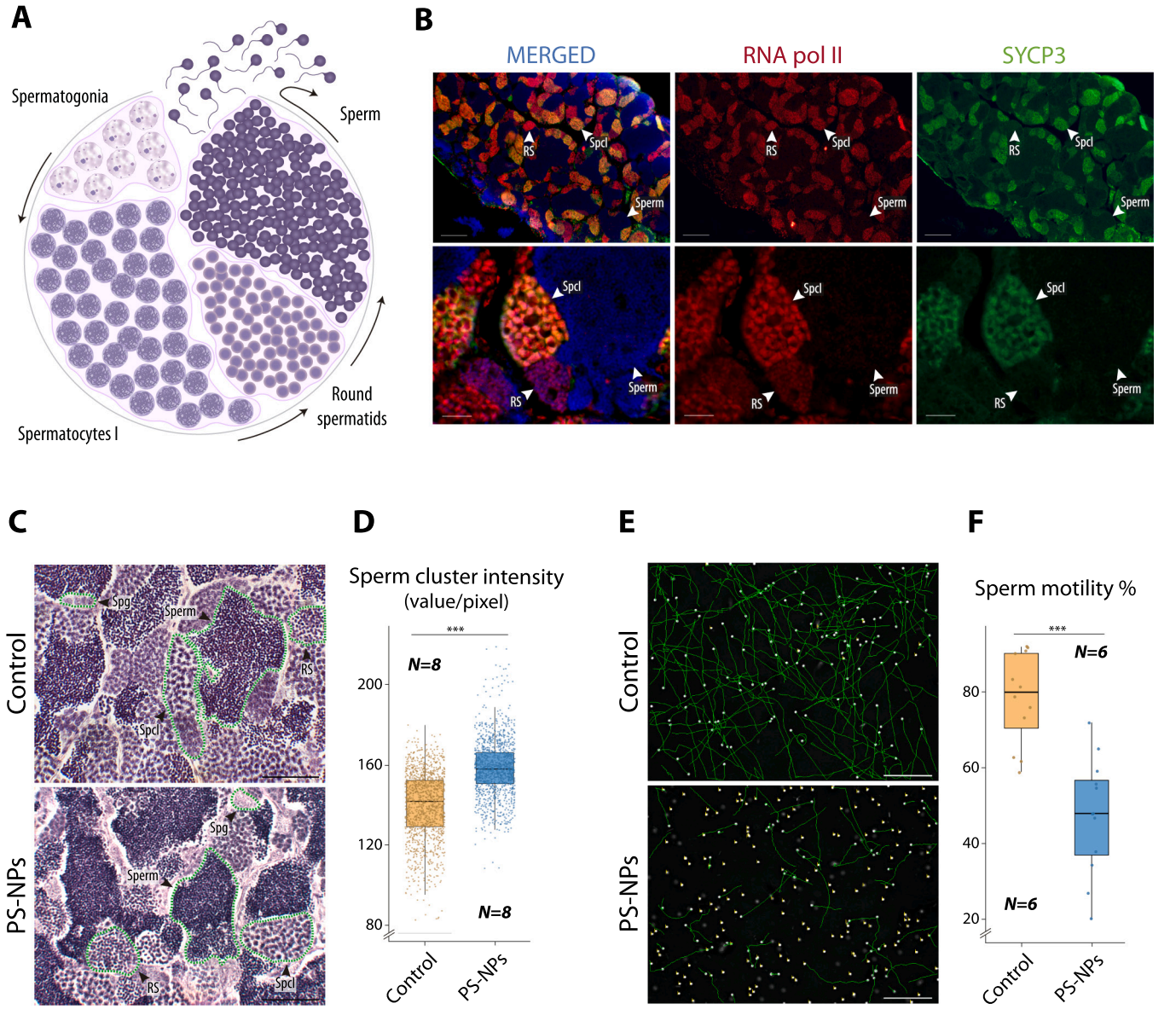

Fig. 1. PS-NPs affect spermatogenesis and sperm motility. **(A)** Schematic representation of spermatogenesis in zebrafish. Note how the spermatogenesis cycle is organized into cysts. **(B)** Immunofluorescence images representing testis cysts using antibodies against RNApol II (red) and SYCP3 (green). DNA is counter stained with DAPI (blue). Scale bar 50 μm. According to staining patterns, different cell types can be distinguished: primary spermatocytes (SpcI), round spermatids (RS) and sperm. **(C)** Histological sections of control (upper panel) and PS-NPs exposed (lower panel) from adult zebrafish individuals stained with PAS-Hematoxylin. Scale bar 20 μm. **(D)** Boxplot representing the sperm median intensity (as value per pixels) ± SD for each measured cluster in both conditions (two-way ANOVA, ***$p < 0.001$). A total of 1292 control sperm clusters and 1259 plastic sperm clusters were included in the analysis. Eight animals were analyzed ($N = 8$), representing four replicates. **(E)** Microscopical images of spermatic water activated samples from control individuals (upper panel) and PS-NPs exposed (lower panel). Each white dot corresponds to a sperm cell whereas each green line shows its trajectory in a specific time. No-motile sperm cells are marked with a yellow sign. Scale bar 50 μm. **(F)** Boxplot showing the CASA calculated sperm motility percentage median ± SD for each condition (two-way ANOVA, ***$p < 0.001$). Six animals were analyzed, representing two replicates.

Further analysis of fixed testis by PAS-Hematoxylin staining, revealed an altered histological organization of testicular cysts following acute exposure to PS-NPs. This was translated into increased levels of sperm clustering in animals exposed to PS-NPs when compared to controls (Fig. 1C-D). Particularly, we detected high levels of sperm clustering intensity (expressed as value per pixel) in PS-NPs-exposed male fish (p-value $< 2e^{-16}$, two-way ANOVA). These results were indicative of an alteration of chromatin compaction in later stages of spermatogenesis that might affect sperm viability. In fact, when analyzing spermatozoa concentration and motility by CASA we detected statistically significant reduction (p-value $= 1.73e^{-5}$, two-way ANOVA) in sperm motility in PS-NPs-exposed male fish (Fig. 1E-F).

3.2. Internalization of PS-NPs in male germ cells

We subsequently examined the bioavailability of the nanoparticles by flow cytometry to determine whether the observed germline effects were the results of a direct or indirect response (Fig. 2). Our results clearly show that the effects were directly attributable to the interaction of nanoplastics with the gonads. Specifically, labeled PS-NPs were found to penetrate the testicular barrier. This was evidenced by an increase in green fluorescence in both, cells and spectrum of exposed individuals when compared to the control (Fig. 2A-B), with a 4.90 % of living cells in the exposed sample showing a positive profile for Dragon-Green. Cytometry imaging further revealed that the nanoparticles not only crossed the testicular barrier but were also internalized within germline cells. This was confirmed by the presence of green fluorescent cells of varying sizes in the exposed sample (Fig. 2C). Further enrichment analysis of sorted cells using immunostaining revealed differences between cell types present in the population positive for Dragon-Green when compared to controls (p-value = 0.00035, Chi-square test), indicating that the labeled nanoparticles were not equally internalized by all cell types. Specifically, when comparing the negative PS-NPs and positive PS-NPs populations, significant differences (p-value = 1.82e-6, Chi-square test) were observed. Larger and less compact spermatogenic cell types (spermatocytes I) showed greater internalization of the labeled particles, with spermatocytes I representing 17.01 % of the negative control sample and 39.17 % of the positive PS-NPs exposed sample (Fig. 2D). Altogether, our results demonstrate that the observed germline effects were directly due to nanoplastics penetrating the testicular barrier and being internalized within germline cells, more specifically in primary spermatocytes.

3.3. Acute exposure to PS-NPs induces apoptosis and increases meiotic DNA repair

We next evaluated levels of germ cell apoptosis upon PS-NPs exposure by caspase-3 staining. We found that acute exposure to PS-NPs results in high levels of caspase-3 positive cells per spermatocyte clusters (p-value = 0.029, Chi-square test) (Fig. 3A-C), indicative of cell apoptosis occurring during prophase I. Given the elevated germ cell apoptosis and germline chromosome organization defects observed during pachytene, we examined whether PS-NPs exposure causes defects in DNA double-strand breaks (DSBs) during prophase I. We quantified

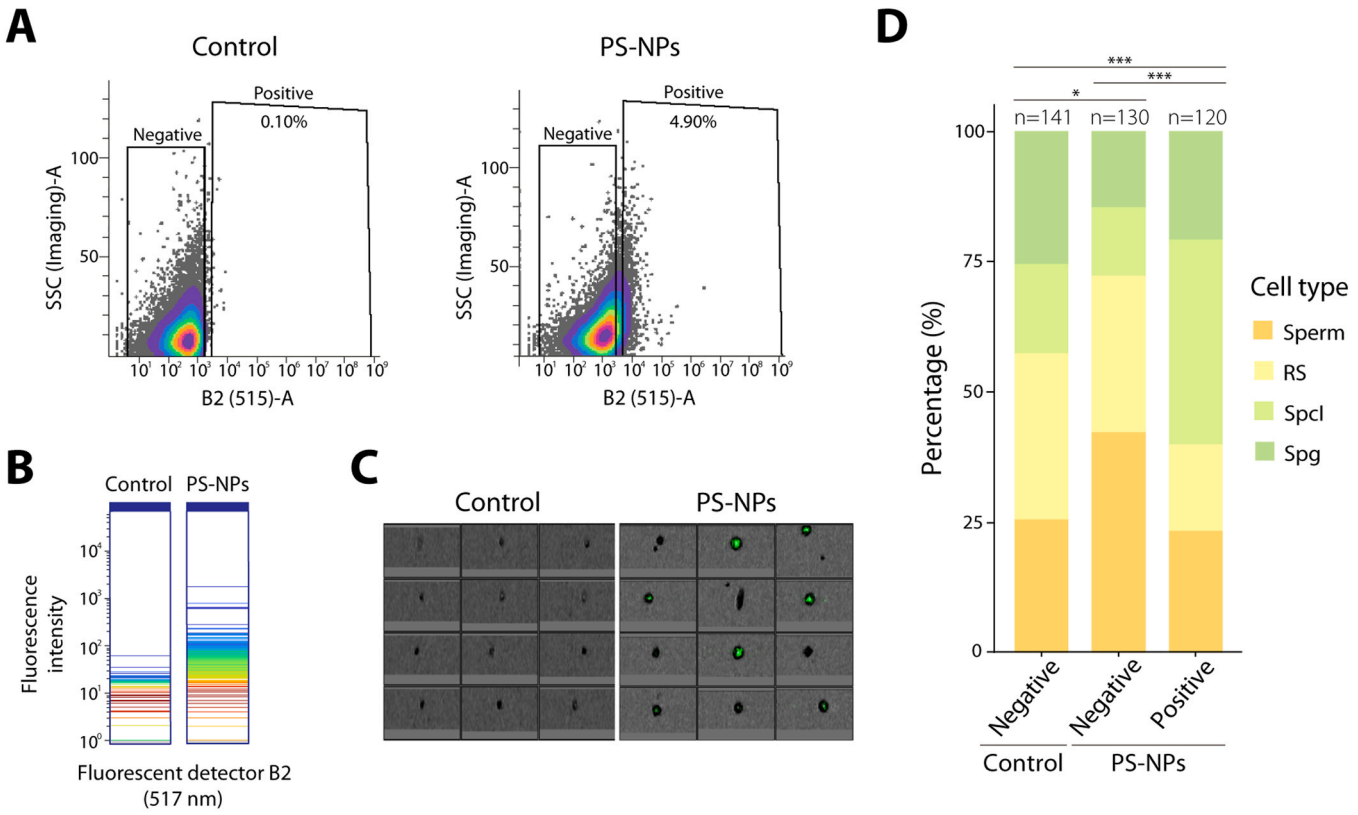

Fig. 2. Internalization of PS-NPs in male germ cells. Cytometer profiles and enrichment analysis resulting from the sorting of testicular disaggregated samples from both control and labeled PS-NPs exposed individuals. **(A)** Control and PS-NPs cytometer scatter plot showing positive and negative cells for Dragon-Green fluorescent particles. Scatter plot axes represent B2 detector (B2 (515)-A), to identify positive cells for the fluorochrome, versus side scatter (SSC (Imaging)-A), which organizes cells depending on their complexity. **(B)** Spectral plot for B2 fluorochrome detector (517 nm) showing the density of the events by intensity for this specific detector in control and PS-NPs samples. **(C)** Cytometry imaging of the sorted populations, selecting the parameters LightLoss (Imaging) and Dragon-Green fluorochrome detector for both control (negative population) and PS-NPs (positive population) samples. **(D)** Enrichment analysis bar plot for the sorted populations representing the percentage of each spermatogenic cell type (Sperm; RS: round spermatids; SpcI: spermatocytes I; Spg: spermatogonia) in different populations (Control negative, PS-NPs negative and PS-NPs positive) (Chi-square, *p < 0.05, ***p < 0.001). A total of 120–140 cells were analyzed for each population.

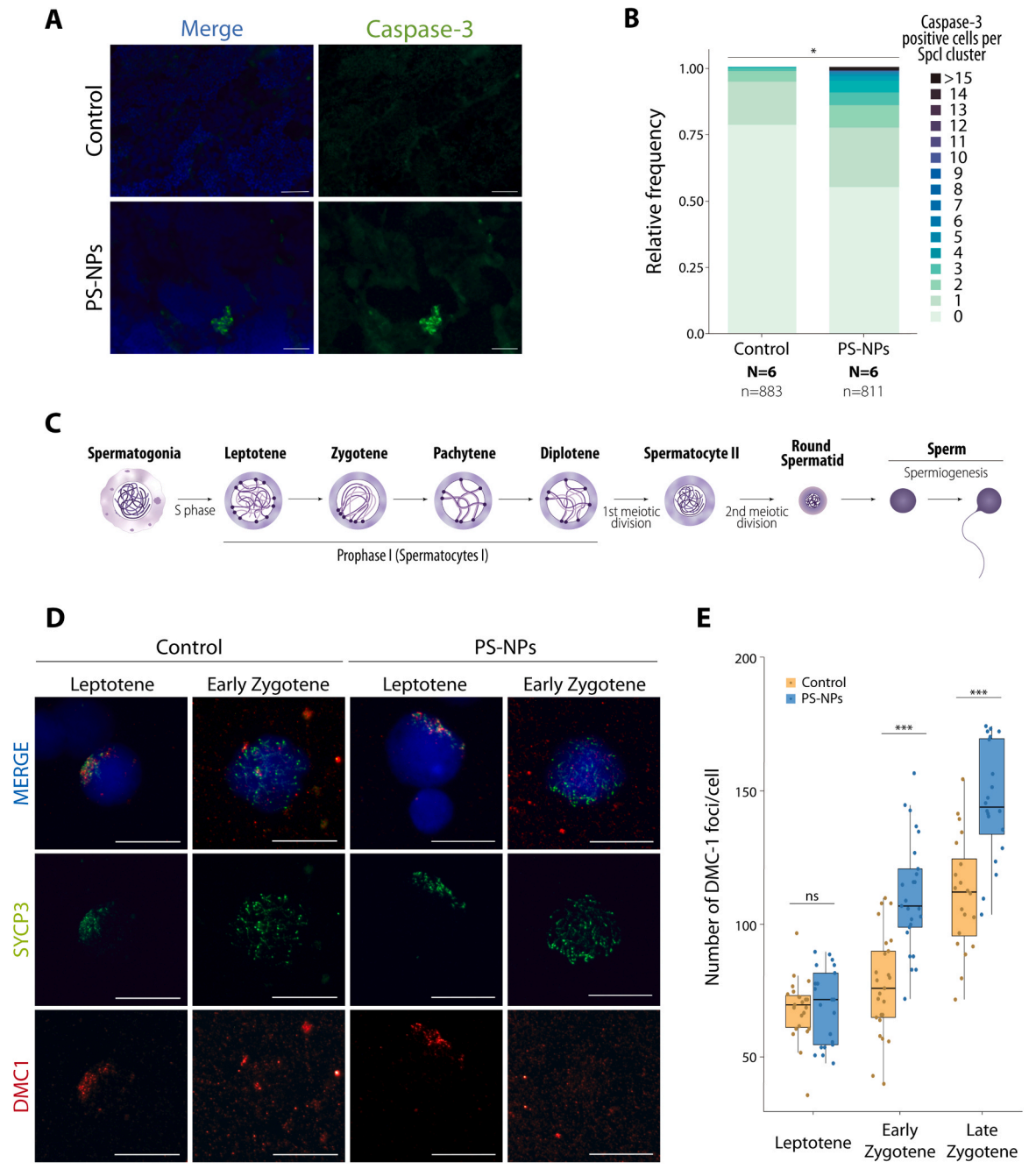

Fig. 3. PS-NPs induce germ cell apoptosis and meiotic double strand-breaks **(A)** Immunofluorescence images of control (upper panel) and PS-NPs exposed (lower panel) adult zebrafish males using caspase-3 (green), DNA counter stained with DAPI (blue). Each green dot corresponds to a caspase-3 positive spermatocyte I cell. Scale bar 50 μm. **(B)** Bar chart representation of the relative frequency of caspase-3 positive cells per spermatocyte I testicular cyst (Chi-square, *$p < 0.05$). A total of 883 spermatocyte I control clusters and 811 spermatocyte I plastic exposed clusters were included in the analysis. Six animals were analyzed, representing three replicates. **(C)** Schematic representation of zebrafish spermatogenic process with special emphasis on meiosis and prophase I stages, where recombination takes place. **(D)** Representative immunofluorescence images of primary spermatocytes in different stages of meiosis from control (left panels) and PS-NPs exposed (right panels) adult zebrafish males. Images represent SYCP3 labeling of the chromosomal axes (green) and Dmc1 (red). DNA is counter stained with DAPI (blue). Scale bar 20 μm. **(E)** Boxplot number of DMC1 foci for each cell type and condition (two-way ANOVA, ***$p < 0.001$, ns nonsignificant). Boxplots are presented as median values (center line) ± SD. A total of 68 cells were analyzed for the control (n = 23 for leptotene, n = 25 for early zygotene and n = 20 for late zygotene) and 66 cells were analyzed for the exposed individuals (n = 21 for leptotene, n = 25 for early zygotene and n = 20 for late zygotene).

the levels of foci for the DMC-1 recombinase, an ortholog of human DMC-1 that binds to 3′ ssDNA ends at DSBs to promote strand invasion and exchange for DSB repair [25-27] on immunostained spermatocyte spreads to observe DSB formation and repair progression. In PS-NPs exposed animals, as in controls, we detected low and similar levels of DMC-1 foci in early stages of prophase I (leptotene) (p-value = 0.81, two-way ANOVA). However, as prophase-I progresses, levels of DMC-1 foci were significantly increased in zygotene stages (both early and late) of PS-NPs treated animals compared with control (early zygotene: p-value = $3.62e^{-7}$, two-way ANOVA; late zygotene: p-value = $1.21e^{-5}$, two-way ANOVA) (Fig. 3D-E). These data suggest that exposure to PS-NPs results in an elevated meiotic DSB level. Unrepaired meiotic DSBs can induce the activation of meiotic checkpoints [28], resulting in high levels of apoptosis. Our observations are consistent with this

scenario. Taken together, these results show evidence of increased germ cell apoptosis and high levels of DSB formation after exposure to PS-NPs.

3.4. PS-NPs exposure alters expression of genes regulating meiosis and chromatin structure

To further determine whether the male germline defects observed following PS-NPs exposure might stem from alterations in gene expression, we performed RNA sequencing (RNA-seq) from whole testis comparing control and PS-NPs-exposed male fish (three biological replicates) (Fig. 4A). We detected 2303 statistically significant differentially expressed genes (DEGs) upon NPs exposure (590 up-regulated in exposed individuals and 1713 down-regulated) (Fig. 4B-C), mainly including protein coding genes. Gene ontology (GO) enrichment analysis of the DE genes (Fig. 4D-E) resulted in several top biological processes for up-regulated genes, including meiosis and reproduction. And more specifically, genes involved in the formation and repair of DSBs (DMC-1, RAD54, MSH4 and Trip13, among others), meiotic chromosomal axes assembly and chromatin conformation (Supplementary Table 1). On the other hand, genes involved in fertilization, immune system and cell adhesion were detected as the top biological processes for down-regulated genes (Supplementary Table 1). Concordantly, when interrogating the main affected pathways, fertilization, reproduction and innate immune system were highlighted (Fig. 4F and Supplementary Table 2). Altogether, our results show that PS-NPs exposure induces altered gene expression of a specific set of genes including genes involved in reproduction and chromatin remodeling, as well as innate immune system related genes, which indicates a fast immunologic response within the gonad to phagocyte the nanoparticle with neutrophiles and macrophages.

3.5. Oocyte growth is not severely affected after PS-NPs acute exposure

We further characterized oogenesis progression in zebrafish by using

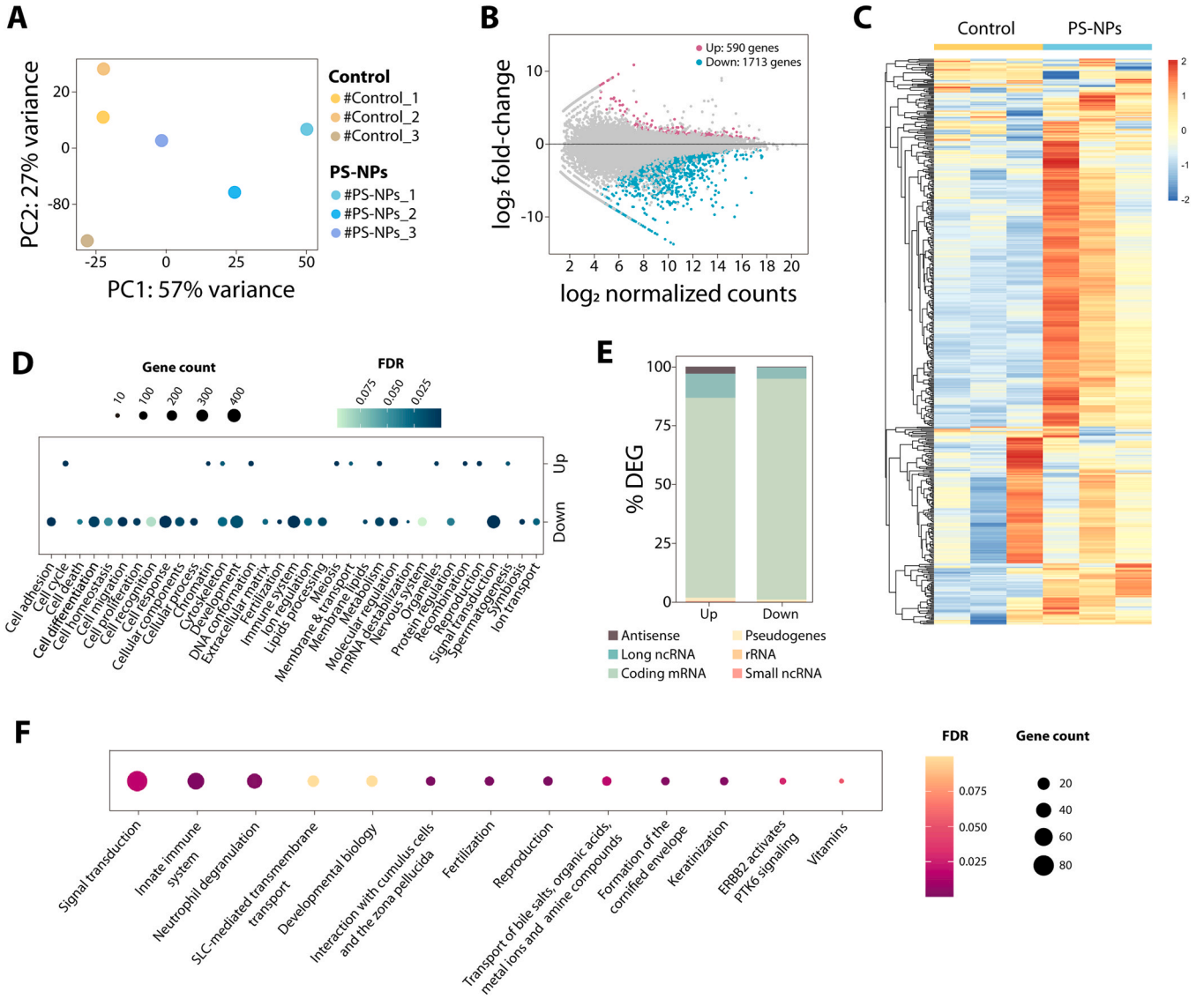

Fig. 4. PS-NPs alter gene expression in males. **(A)** PCA plot including 3 individuals for each condition (control and PS-NPs exposed). **(B)** MAplot representation of up regulated (dark pink) and down regulated (turquoise) genes in PS-NPs exposed individuals (fold-change≥1; FDR<0.1). **(C)** Heat map showing the expression fold change as $\log_2$ for all 500 most differentially expressed genes between control and PS-NPs exposed adult zebrafish testicles. **(D)** Gene Ontology (GO) analysis of all up and down regulated genes showed in panel B. The number of genes assigned to each GO category is represented by the bubble size, whereas the color of the bubbles indicates its FDR. **(E)** Percentage of differentially expressed genes (DEGs) RNA biotype category, including antisense, long non-coding RNA, coding mRNA, pseudogenes, rRNA and small non-coding RNA. **(F)** Reactome pathway analysis of all dysregulated genes showed in panel B. The number of genes assigned to each pathway category is represented by the bubble size, whereas the color of the bubbles indicates its FDR.

topographical staining (i.e., PAS-Hematoxylin) of histological sections of ovaries (Fig. S3A-B). We identified different stages of oogenesis in teleost fishes distinguishing between stage I (primary growth), stage II (cortical alveolus) and stage III (vitellogenesis) according to [8,29]. Stage I was further classified between the pre-follicle phase (stage IA with one nucleolus and multiple nucleoli) and follicle stage (stage IB). Stage II cells we differentiated between early cortical alveoli and late cortical alveoli. Stage III of vitellogenesis corresponded to oocytes in metaphase II arrest.

A detailed histological analysis detected altered relative frequencies of oocytes stages upon PS-NPs acute exposure. We detected alterations in stage IB (23.49 % in controls and 34.46 %in PS-NPs-exposed females) and stage II (29.78 % in controls and 19.43 % in PS-NPs-exposed females) (p-value = $6.65e^{-5}$, Chi-square test) (Fig. S3C), suggesting a delay in oocyte growth. This delay did not affect substantially the relative frequency of oocytes in stage III.

3.6. Fertility assays

Given the distinctive effects of PS-NPs acute exposure in the male and female germline, we conducted fertility assays analyzing different parameters including average laid eggs, cumulative larval survival and hatching, together with heartbeat recording (Fig. 5). We detected a tendency, although not significant (p-value = 0.41, two-way ANOVA) of reduced number of eggs in exposed females (55.5 egg mean in controls and 37.67 egg mean in PS-NPs-exposed females) (Fig. 5A). This was consistent with the unaltered relative frequency of oocytes in stage III (Fig. S3C). However, when analyzing cumulative larval survival, we detected a slight reduction in exposed animals (Fig. 5B). This was accompanied by a delay in larvae hatching (Fig. 5C). Importantly, heartbeat was reduced upon PS-NPs exposure (p-value = 0.0037, two-way ANOVA) (Fig. 5D).

4. Discussion

Our study provides a comprehensive view of the detrimental effects of acute NP exposure on the reproductive system of zebrafish, providing new insights into the molecular pathways impacted by pollutants. Studies conducted so far in zebrafish have been focused on the presence of common development impairments found in embryos exposed to plastic NPs, including morphoanatomical defects, lower hatching rates and alterations of the oxidative stress response, among others [30-32]. And although it has been reported that NPs can bioaccumulate in the maternally and co-parentally exposed F1 embryos/larvae, no major physiological disturbances were detected [33]. However, the fact that PS-NPs could bioaccumulate and be passed on to the offspring called for a potential effect in the germline yet to be determined. Here we demonstrate that, although in different degrees, both the male and female germline can be directly affected upon acute exposure to NPs in zebrafish and their accumulation within the gonadal cells.

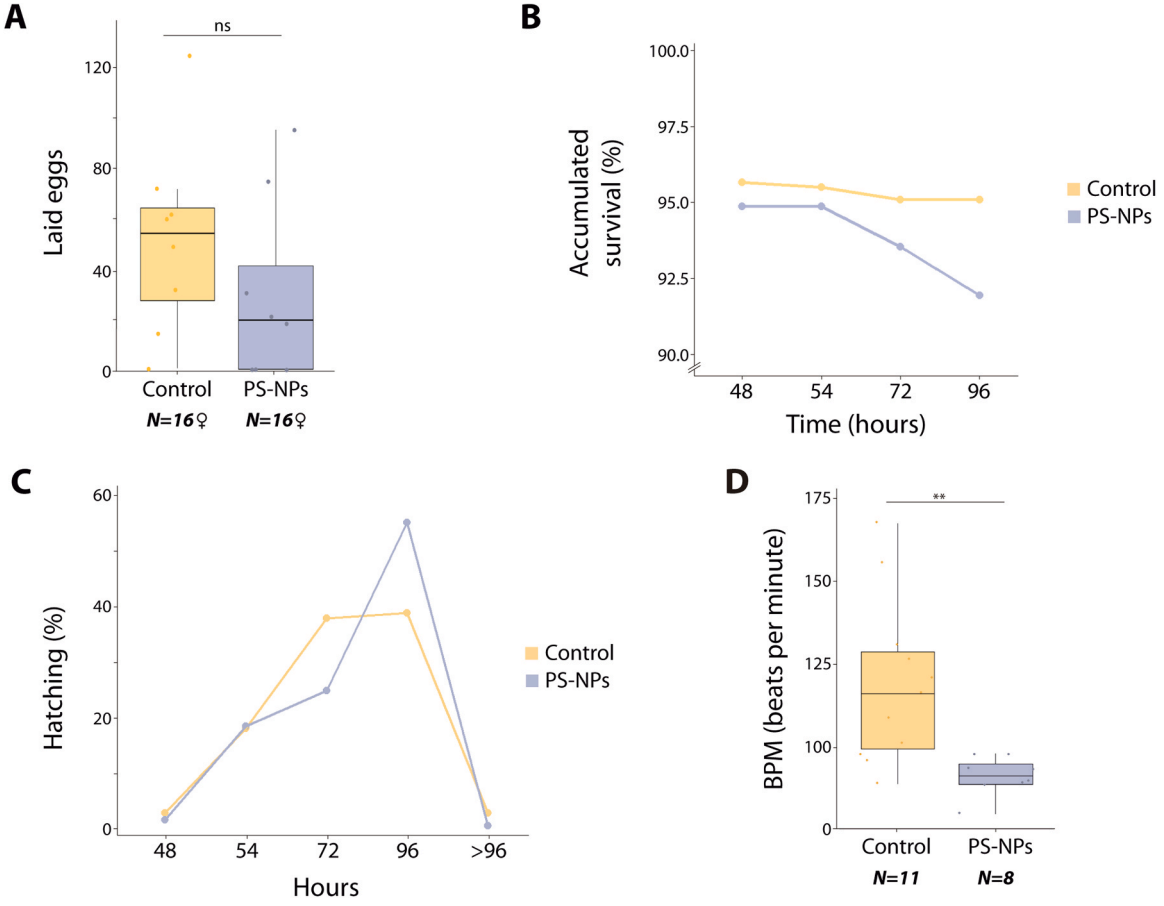

Fig. 5. PS-NPs affect fertility and F1 individual performance. **(A)** Bar chart showing the average number of eggs laid for both conditions (two-way ANOVA, *p < 0.05, ns nonsignificant). Boxplots are presented as median values (center line) ± SD. Sixteen females were analyzed, representing three replicates. **(B)** Scatter plot showing the percentage of fecundated eggs accumulated survival from 48 hpf until 96 hpf for F0 control and F0 PS-NPs exposed descendants (two-way ANOVA, p > 0.05). **(C)** Scatter plot representation of the percentage of eggs hatching at different time points for control and PS-NPs exposed F0 descendants (two-way ANOVA, p > 0.05). **(D)** Boxplot showing F1 larvae heartbeat in bpm (beats per minute) at 7 dpf from individuals resulting from F0 control and PS-NPs exposed individuals (two-way ANOVA, **p < 0.01). Boxplots are presented as median values (center line) ± SD. Eleven control individuals and eight exposed individuals were analyzed, representing two replicates.

Our results indicate that NPs induced changes in the histological distribution and clustering of germ cells within the testis resulting in an increased sperm clustering within the seminiferous tubules when compared to non-exposed animals. In zebrafish, as in other anamniote vertebrates, spermatogenesis occurs in cysts, and the combined duration of meiotic and spermiogenic phases is very short, lasting approximately 6 days [34]. This short cycling allowed to detect changes in the testis after 96 h of exposure of NPs. In fact, we detected alterations in both meiotic (primary spermatocytes) and post-meiotic cells (sperm).

In the case of primary spermatocytes, we detected a high percentage of cells in leptotene stage in exposed animals. This suggested a delay in the progression of prophase I. In fact, meiotic progression involves chromosome movements and chromatin rearrangements that must be carefully regulated to generate healthy gametes. The most critical chromosome movements occurring during the first meiotic prophase include alignment, pairing, synapsis, and recombination between homologs [23,35]. These processes are initiated by the generation of highly programmed DSBs during early stages of prophase I by a plethora of proteins involved in the DSB repair mechanisms such as RAD51 (Recombinase A Homolog 51) and DMC1 (DNA Meiotic Recombinase 1) and others [36,37].

Importantly, meiosis progression is highly regulated and monitored by specific meiotic checkpoints [38-41], including: i) response to unrepaired DSBs; ii) meiotic silencing of unsynapsed chromatin; and iii) spindle assembly checkpoint (reviewed in [41]). The first meiotic checkpoint is triggered as a response to unrepaired meiotic DSBs. In this context, the observed high rate of apoptosis involving primary spermatocytes detected in males exposed to NPs suggest the activation of this mechanism. This was supported by the observation of high number of DMC1 foci in zygotene stages upon exposure of NPs. In fact, testes from exposed animals showed a distinct transcriptional identity, with high transcriptional levels of genes involved in the formation and repair of meiotic DSBs, including Trip13, DMC1 and MSH4, among others. Our results are in consonance with previous reports on the increase of DSB upon pollutants in different systems, such as *C. elegans* [42].

Alterations of the meiotic progression and DNA repair were also accompanied by changes in chromatin compaction in post-meiotic cells (sperm). This was supported by both histological observations and transcriptional profiling as genes involved in DNA condensation and nucleosome assembly were mainly upregulated upon NP exposure and although we detected viable spermatozoa, they showed reduced motility suggesting functional impairment. In fact, previous studies exposing rodents to microplastics have reported poor sperm quality and quantity [43-46], although the underlying mechanisms remained unknown. One possibility can be oxidative stress, as different genes related to an increase in oxidative stress (foxo3b, fosab, mapk12a or jun) have been shown to be dysregulated after the exposure. Since NPs can increase oxidative stress in the body, involving an imbalance between free radicals and antioxidants, this could lead to cell and tissue injury. In the context of spermatogenesis, this could lead to DNA damage. Our observations indicate that NPs can induce profound alterations of the genome architecture of male germ cells, ultimately affecting sperm quality. All these effects can act synergically with inflammation, which can be caused upon exposure to NPs [47-49]. Accordantly, we detected a downregulation of genes involved in the inflammatory response.

The effects observed in zebrafish females were mild as oocyte maturation was not severely affected after PS-NPs acute exposure, mirroring previous lack of effect on the ovarian index [50]. In fact, it has been proposed that the potency of the granulosa and cumulus cells, in addition to the extracellular matrix that surrounds the oocyte, to temper and prevent the exposure of the oocyte to MNPs is an important factor to consider [51]. This could indicate that not only the size, but also the type of plastic may have a distinct impact on the outcome for ovarian exposure.

5. Conclusions

Collectively, our results demonstrate the presence of germline dysfunction following acute exposure to NPs in zebrafish. The implications of these findings are profound, with implications for reproductive health and environmental risk assessment. First, they show that short-acute exposure to NPs can already result in histopathological changes in testis, affecting sperm motility. Although previous studies have reported histological abnormalities in rodents [52] our results underscore the importance of considering short exposures in aquatic ecosystems, which are especially sensitive to pollutants. Second, they pinpoint to an interplay of different molecular pathways impacted by pollutants. To the previously described role of the immune system, here we add new genetic pathways involved in DNA formation and repair, and chromatin remodeling. All in all, our study provides an example of how acute exposure to NPs can compromise reproductive fitness in both males and females, providing new insights into the molecular pathways involved. These findings emphasize the urgent need for regulatory actions to limit NP pollution and call for further research in ecotoxicology and reproductive biology to better understand the long-term impacts on aquatic life and ecosystem health.

Environmental implications

This study underscores the escalating environmental concern of nanoplastic pollution, whose impacts on biodiversity and human health are yet to be fully understood. This is especially relevant in aquatic ecosystems where nanoplastics are teeming with life. Our findings reveal that short-term exposure to nanoplastics can induce alterations in the germline of zebrafish, affecting both male and female reproductive processes. These alterations, linked to changes in gene expression, can compromise reproductive fitness, highlighting the potential environmental and health impacts of plastic pollution.

Funding

This work was supported by the Spanish Ministry of Science and Innovation (PID2020–112557GB-I00 founded by AEI/10.13039/501100011033 to A.R.-H.; PID2021–126710OB-C21 to N.R.A; and PID2022–138066OB-I00 to J.C. and PID2020–113221RB-I00 to M.T), the Agència de Gestió d'Ajuts Universitaris i de Recerca, AGAUR (2021SGR00122 to A.R.-H. and 2021SGR00068 to J.C) and the Catalan Institution for Research and Advanced Studies (ICREA) to A.R.-H. G.P. and L.A.-G. were supported by FPI predoctoral fellowships from the Ministry of Economy and Competitiveness (PRE-C-2021–0083 and PRE-2018–083257, respectively). L.M.-G. was supported by an FPU predoctoral fellowship from the Ministry of Science, Innovation and University (FPU18/03867). MT was supported by a Ramon y Cajal contract (ref. RYC2019–026841-I).

CRediT authorship contribution statement

Nerea Roher: Writing – review & editing, Validation, Resources, Methodology, Funding acquisition, Formal analysis. **Aurora Ruiz-Herrera:** Writing – review & editing, Writing – original draft, Validation, Supervision, Resources, Methodology, Funding acquisition, Conceptualization. **Joan Cerda:** Writing – review & editing, Resources, Funding acquisition, Formal analysis. **Mariana Teles:** Writing – review & editing, Formal analysis. **François Chauvigné :** Validation, Methodology. **Laura Gonzalez-Rodelas:** Validation, Methodology. **Lucía Álvarez-González:** Methodology. **Gala Pujol:** Writing – review & editing, Writing – original draft, Validation, Methodology, Formal analysis. **Laia Marin-Gual:** Validation, Methodology.

Declaration of Competing Interest

The authors declare that they have no known competing financial interests or personal relationships that could have appeared to influence the work reported in this paper.

Acknowledgments

Authors thank Egle Kelpsiene, Alexander Goikoetxea and Irene Brandts for the technical support and Manuela Costa for her technical support during flow cytometry. Authors also thank Dr. Yukiko Imai and Dr. Noriyoshi Sakai from the National Institute of Genetics (Japan) for kindly supplying the guinean pig anti-Dmc1 antibody.

Appendix A. Supporting information

Supplementary data associated with this article can be found in the online version at doi:10.1016/j.jhazmat.2024.136529.

Data availability

RNA-sequencing data generated during this study can be found at NCBI Gene Expression Omnibus (GEO) under accession number GSE279916.

References

[1] Rochman, C.M., Cook, A.M., Koelmans, A.A., 2016. Plastic debris and policy: using current scientific understanding to invoke positive change. Environ Toxicol Chem 35 (7), 1617–1626. https://doi.org/10.1002/etc.3408.

[2] Katsumiti, A., Losada-Carrillo, M.P., Barros, M., Cajaraville, M.P., 2021. Polystyrene nanoplastics and microplastics can act as Trojan horse carriers of benzo(a)pyrene to mussel hemocytes in vitro. Sci Rep 11 (1). https://doi.org/10.1038/s41598-021-01938-4.

[3] Menéndez-Pedriza, A., Jaumot, J., 2020. Interaction of environmental pollutants with microplastics: a critical review of sorption factors, bioaccumulation and ecotoxicological effects. Toxics 8 (2), 40. https://doi.org/10.3390/TOXICS8020040.

[4] Trevisan, R., Uzochukwu, D., Di Giulio, R.T., 2020. PAH sorption to nanoplastics and the trojan horse effect as drivers of mitochondrial toxicity and PAH localization in zebrafish. Front Environ Sci 8, 78. https://doi.org/10.3389/fenvs.2020.00078.

[5] Fleury, J.-B., Baulin, V.A., 2021. Microplastics destabilize lipid membranes by mechanical stretching. Proc Natl Acad Sci U S A 118 (31), e2104610118. https://doi.org/10.1073/pnas.2104610118.

[6] Alix, M., Kjesbu, O.S., Anderson, K.C., 2020. From gametogenesis to spawning: how climate-driven warming affects teleost reproductive biology. In: Journal of Fish Biology, 97, pp. 607–632. https://doi.org/10.1111/jfb.14439.

[7] Kagawa, H., Sakurai, Y., Horiuchi, R., Kazeto, Y., Gen, K., Imaizumi, H., et al., 2013. Mechanism of oocyte maturation and ovulation and its application to seed production in the Japanese eel. In: Fish Physiology and Biochemistry, 39, pp. 13–17. https://doi.org/10.1007/s10695-012-9607-3.

[8] Lubzens, E., Young, G., Bobe, J., Cerdà, J., 2010. Oogenesis in teleosts: how fish eggs are formed. Gen Comp Endocrinol 165 (3), 367–389. https://doi.org/10.1016/j.ygcen.2009.05.022.

[9] Schulz, R.W., de França, L.R., Lareyre, J.J., LeGac, F., Chiarini-Garcia, H., Nobrega, R.H., et al., 2010. Spermatogenesis in fish. Gen Comp Endocrinol 165 (3), 390–411. https://doi.org/10.1016/j.ygcen.2009.02.013.

[10] Sousa, A.L., Campos-Junior, P.H.A., Costa, G.M.J., de França, L.R., 2014. Spermatogenic cycle length and sperm production in the freshwater turtle Kinosternon scorpioides. Biol Reprod 90 (2). https://doi.org/10.1095/biolreprod.113.112391.

[11] Amereh, F., Babaei, M., Eslami, A., Fazelipour, S., Rafiee, M., 2020. The emerging risk of exposure to nano(micro)plastics on endocrine disturbance and reproductive toxicity: from a hypothetical scenario to a global public health challenge. Environ Pollut 261, 114158. https://doi.org/10.1016/j.envpol.2020.114158.

[12] Jaikumar, G., Brun, N.R., Vijver, M.G., Bosker, T., 2019. Reproductive toxicity of primary and secondary microplastics to three cladocerans during chronic exposure. Environ Pollut 249, 638–646. https://doi.org/10.1016/j.envpol.2019.03.085.

[13] Park, E.J., Han, J.S., Park, E.J., Seong, E., Lee, G.H., Kim, D.W., et al., 2020. Repeated-oral dose toxicity of polyethylene microplastics and the possible implications on reproduction and development of the next generation. Toxicol Lett 324, 75–85. https://doi.org/10.1016/j.toxlet.2020.01.008.

[14] Rist, S., Baun, A., Hartmann, N.B., 2017. Ingestion of micro- and nanoplastics in Daphnia magna – Quantification of body burdens and assessment of feeding rates and reproduction. Environ Pollut 228, 398–407. https://doi.org/10.1016/j.envpol.2017.05.048.

[15] Trifuoggi, M., Pagano, G., Oral, R., Pavičić-Hamer, D., Burić, P., Kovačić, I., et al., 2019. Microplastic-induced damage in early embryonal development of sea urchin Sphaerechinus granularis. Environ Res 179, 108815. https://doi.org/10.1016/j.envres.2019.108815.

[16] Avdesh, A., Chen, M., Martin-Iverson, M.T., Mondal, A., Ong, D., Rainey-Smith, S., et al., 2012. Regular care and maintenance of a Zebrafish (Danio rerio) laboratory: an introduction. J Vis Exp (69). https://doi.org/10.3791/4196.

[17] Brandts, I., Cánovas, M., Tvarijonaviciute, A., Llorca, M., Vega, A., Farré, M., et al., 2022. Nanoplastics are bioaccumulated in fish liver and muscle and cause DNA damage after a chronic exposure. Environ Res 212, 113433. https://doi.org/10.1016/j.envres.2022.113433.

[18] Capilla, L., Medarde, N., Alemany-Schmidt, A., Oliver-Bonet, M., Ventura, J., Ruiz-Herrera, A., 2014. Genetic recombination variation in wild Robertsonian mice: on the role of chromosomal fusions and Prdm9 allelic background. Proc R Soc B: Biol Sci 281 (1786). https://doi.org/10.1098/rspb.2014.0297.

[19] Garcia-Cruz, R., Pacheco, S., Brieño, M.A., Steinberg, E.R., Mudry, M.D., Ruiz-Herrera, A., et al., 2011. A comparative study of the recombination pattern in three species of Platyrrhini monkeys (Primates). Chromosoma 120 (5), 521–530. https://doi.org/10.1007/s00412-011-0329-6.

[20] Marín-Gual, L., González-Rodelas, L., Pujol, G., Vara, C., Martín-Ruiz, M., Berríos, S., et al., 2022. Strategies for meiotic sex chromosome dynamics and telomeric elongation in Marsupials. PLOS Genet 18. https://doi.org/10.1371/journal.pgen.1010040.

[21] Raghunath, A., Perumal, E., 2018. Analysis of lethality and malformations during zebrafish (Danio rerio) development. In: Methods in Molecular Biology, 1797. Humana Press Inc,, pp. 337–363. https://doi.org/10.1007/978-1-4939-7883-0_18.

[22] Brandts, I., Garcia-Ordoñez, M., Tort, L., Teles, M., Roher, N., 2020. Polystyrene nanoplastics accumulate in ZFL cell lysosomes and in zebrafish larvae after acute exposure, inducing a synergistic immune response: In vitro without affecting larval survival in vivo. Environ Sci: Nano 7 (8), 2410–2422. https://doi.org/10.1039/d0en00553c.

[23] Vara, C., Paytuví-Gallart, A., Cuartero, Y., Le Dily, F., Garcia, F., Salvà-Castro, J., et al., 2019. Three-dimensional genomic structure and cohesin occupancy correlate with transcriptional activity during spermatogenesis. Cell Rep 28 (2), 352–367.e9. https://doi.org/10.1016/j.celrep.2019.06.037.

[24] Imai, Y., Olaya, I., Sakai, N., Burgess, S.M., 2021. Meiotic chromosome dynamics in zebrafish, 9. Frontiers in Cell and Developmental Biology. https://doi.org/10.3389/fcell.2021.757445.

[25] Brick, K., Pratto, F., Sun, C.Y., Camerini-Otero, R.D., Petukhova, G., 2018. Analysis of meiotic double-strand break initiation in mammals, 601. Methods in Enzymology, pp. 391–418. https://doi.org/10.1016/bs.mie.2017.11.037.

[26] Chan, Y.L., Zhang, A., Weissman, B.P., Bishop, D.K., 2019. RPA resolves conflicting activities of accessory proteins during reconstitution of Dmc1-mediated meiotic recombination. Nucleic Acids Res 47 (2), 747–761. https://doi.org/10.1093/nar/gky1160.

[27] Davies, B., Zhang, G., Moralli, D., Alghadban, S., Biggs, D., Preece, C., et al., 2023. Characterization of meiotic recombination intermediates through gene knockouts in founder hybrid mice. Genome Res 33 (11), 2018–2027. https://doi.org/10.1101/gr.278024.123.

[28] A. Gartner S. Milstein S. Ahmed J. Hodgkin M.O. Hengartner. Weinert, 1998; Caspari and Carr. In Lydall and Weinert (Vol. 5). 2000.

[29] Selman, K., Wallace, R.A., Sarka, A., Qi, X., 1993. Stages of oocyte development in the zebrafish. Brachydanio rerio. J Morphol 218 (2), 203–224.. https://doi.org/10.1002/jmor.1052180209.

[30] Lee, C.Y., Horng, J.L., Chen, P.Y., Lin, L.Y., 2019. Silver nanoparticle exposure impairs ion regulation in zebrafish embryos. Aquat Toxicol 214, 105263. https://doi.org/10.1016/j.aquatox.2019.105263.

[31] Santos, D., Félix, L., Luzio, A., Parra, S., Cabecinha, E., Bellas, J., et al., 2020. Toxicological effects induced on early life stages of zebrafish (Danio rerio) after an acute exposure to microplastics alone or co-exposed with copper. Chemosphere 261, 127748. https://doi.org/10.1016/j.chemosphere.2020.127748.

[32] Savuca, A., Nicoara, M.N., Ciobica, A., Gorgan, D.L., Ureche, D., Balmus, I.M., 2023. Current aspects on the plastic nano- and microparticles toxicity in zebrafish—focus on the correlation between oxidative stress responses and neurodevelopment, 13. Animals. https://doi.org/10.3390/ani13111810.

[33] Pitt, J.A., Trevisan, R., Massarsky, A., Kozal, J.S., Levin, E.D., Di Giulio, R.T., 2018. Maternal transfer of nanoplastics to offspring in zebrafish (Danio rerio): a case study with nanopolystyrene. Sci Total Environ 643, 324–334. https://doi.org/10.1016/j.scitotenv.2018.06.186.

[34] Leal, M.C., de Waal, P.P., García-López, Á., Chen, S.X., Bogerd, J., Schulz, R.W., 2009. Zebrafish primary testis tissue culture: an approach to study testis function ex vivo. Gen Comp Endocrinol 162 (2), 134–138. https://doi.org/10.1016/j.ygcen.2009.03.003.

[35] Reig-Viader, R., Garcia-Caldés, M., Ruiz-Herrera, A., 2016. Telomere homeostasis in mammalian germ cells: a review, 125. Chromosoma, pp. 337–351. https://doi.org/10.1007/s00412-015-0555-4.

[36] Hinch, A.G., Becker, P.W., Li, T., Moralli, D., Zhang, G., Bycroft, C., et al., 2020. The configuration of RPA, RAD51, and DMC1 binding in meiosis reveals the nature of critical recombination intermediates. Mol Cell 79 (4), 689–701.e10. https://doi.org/10.1016/j.molcel.2020.06.015.

[37] Li, P., Jin, H., Yu, H.G., 2014. Condensin suppresses recombination and regulates double-strand break processing at the repetitive ribosomal DNA array to ensure proper chromosome segregation during meiosis in budding yeast. Mol Biol Cell 25 (19), 2934–2947. https://doi.org/10.1091/mbc.E14-05-0957.

[38] Bolcun-Filas, E., Handel, M.A., 2018. Meiosis: the chromosomal foundation of reproduction. In: Biology of Reproduction, 99, pp. 112–126. https://doi.org/10.1093/biolre/ioy021.
[39] Handel, M.A., Schimenti, J.C., 2010. Genetics of mammalian meiosis: regulation, dynamics and impact on fertility. *Nat Rev Genet* 11 (2), 124–136. https://doi.org/10.1038/nrg2723.
[40] Jan, S.Z., Jongejan, A., Korver, C.M., van Daalen, S.K.M., van Pelt, A.M.M., Repping, S., et al., 2018. Distinct prophase arrest mechanisms in human male meiosis. Development 145 (16), dev160614. https://doi.org/10.1242/dev.160614.
[41] Subramanian, V.V., Hochwagen, A., 2014. The meiotic checkpoint network: step-by-step through meiotic prophase. Cold Spring Harb Perspect Biol 6 (10), a016675. https://doi.org/10.1101/cshperspect.a016675.
[42] Shin, N., Lascarez-Lagunas, L.I., Henderson, A.L., Martínez-García, M., Karthikraj, R., Barrera, V., et al., 2024. Altered gene expression linked to germline dysfunction following exposure to DEET. IScience 27 (1). https://doi.org/10.1016/j.isci.2023.108699.
[43] Deng, Y., Yan, Z., Shen, R., Huang, Y., Ren, H., Zhang, Y., 2021. Enhanced reproductive toxicities induced by phthalates contaminated microplastics in male mice (Mus musculus). J Hazard Mater 406. https://doi.org/10.1016/j.jhazmat.2020.124644.
[44] Ijaz, M.U., Shahzadi, S., Samad, A., Ehsan, N., Ahmed, H., Tahir, A., et al., 2021. Dose-dependent effect of polystyrene microplastics on the testicular tissues of the male sprague dawley rats. Dose-Response 19 (2). https://doi.org/10.1177/15593258211019882.
[45] Jin, H., Ma, T., Sha, X., Liu, Z., Zhou, Y., Meng, X., et al., 2021. Polystyrene microplastics induced male reproductive toxicity in mice. J Hazard Mater 401. https://doi.org/10.1016/j.jhazmat.2020.123430.
[46] Zhang, C., Chen, J., Ma, S., Sun, Z., Wang, Z., 2022. Microplastics may be a significant cause of male infertility. American Journal of Men's Health 16 (6), 15579883221096549.. https://doi.org/10.1177/15579883221096549.
[47] Guanglin, L., Shuqin, W., 2024. Polystyrene nanoplastics exposure causes inflammation and death of esophageal cell. Ecotoxicol Environ Saf 269. https://doi.org/10.1016/j.ecoenv.2023.115819.
[48] Sangkham, S., Faikhaw, O., Munkong, N., Sakunkoo, P., Arunlertaree, C., Chavali, M., et al., 2022. A review on microplastics and nanoplastics in the environment: their occurrence, exposure routes, toxic studies, and potential effects on human health. Marine Pollution Bulletin 181. https://doi.org/10.1016/j.marpolbul.2022.113832.
[49] Xie, S., Zhou, A., Wei, T., Li, S., Yang, B., Xu, G., et al., 2021. Nanoplastics induce more serious microbiota dysbiosis and inflammation in the gut of adult zebrafish than microplastics. Bull Environ Contam Toxicol 107 (4), 640–650. https://doi.org/10.1007/s00128-021-03348-8.
[50] He, J., Yang, X., Liu, H., 2021. Enhanced toxicity of triphenyl phosphate to zebrafish in the presence of micro- and nano-plastics. Sci Total Environ 756, 143986. https://doi.org/10.1016/j.scitotenv.2020.143986.
[51] Yang, J., Kamstra, J., Legler, J., Aardema, H., 2023. The impact of microplastics on female reproduction and early life. Anim Reprod 20 (2), e20230037. https://doi.org/10.1590/1984-3143-AR2023-0037.
[52] Sharma, K., Sharma, A., Bhatnagar, P., 2024. Combined effect of polystyrene nanoplastic and di-n-butyl phthalate on testicular health of male Swiss albino mice: analysis of sperm-related parameters and potential toxic effects. Environ Sci Pollut Res 31 (16), 23680–23696. https://doi.org/10.1007/s11356-024-32697-0.